Letter

Stabilization of a nonlinear magnonic bullet coexisting with a Bose-Einstein condensate in a rapidly cooled magnonic system driven by spin-orbit torque

Michael Schneider,[1,*] David Breitbach,[1] Rostyslav O. Serha,[1] Qi Wang,[2] Morteza Mohseni,[1] Alexander A. Serga,[1] Andrei N. Slavin,[3] Vasyl S. Tiberkevich,[3] Björn Heinz,[1] Thomas Brächer,[1] Bert Lägel,[1] Carsten Dubs,[4] Sebastian Knauer,[2] Oleksandr V. Dobrovolskiy,[2] Philipp Pirro,[1] Burkard Hillebrands,[1] and Andrii V. Chumak[2]

[1]*Fachbereich Physik and Landesforschungszentrum OPTIMAS, Technische Universität Kaiserslautern, D-67663 Kaiserslautern, Germany*

[2]*Faculty of Physics, University of Vienna, A-1090 Vienna, Austria*

[3]*Department of Physics, Oakland University, Rochester, Michigan 48309, USA*

[4]*INNOVENT e.V. Technologieentwicklung, D-07745 Jena, Germany*

(Received 29 June 2021; accepted 20 September 2021; published 11 October 2021)

We have recently shown that injection of magnons into a magnetic dielectric via the spin-orbit torque (SOT) effect in the adjacent layer of a heavy metal subjected to the action of short (0.1 μs) current pulses allows for control of a magnon Bose-Einstein condensate (BEC). Here, the BEC was formed in the process of rapid cooling (RC), when the electric current heating the sample is abruptly terminated. In the present Letter, we show that the application of a longer (1.0 μs) electric current pulse triggers the formation of a nonlinear localized magnonic bullet below the linear magnon spectrum. After pulse termination, the magnon BEC, as before, is formed at the bottom of the linear spectrum, but the nonlinear bullet continues to exist, stabilized for an additional 30 ns by the same process of RC-induced magnon condensation. Our results suggest that a stimulated condensation of excess magnons to all highly populated magnonic states occurs.

DOI: 10.1103/PhysRevB.104.L140405

Recent experiments in magnon spintronics [1] make use of the magnon injection using spin-polarized currents, which originates from the spin-transfer torque (STT) effect [2,3], and may lead to the excitation of auto-oscillations [4–7] of the low-energy magnon states exhibiting the lowest thresholds for damping compensation. Further studies found the formation of a distinct nonlinear auto-oscillating mode with a frequency below the linear magnon spectrum [8]. This low-frequency mode is identified as a soliton mode, referred to as the bullet mode, and observed in various STT-driven magnon systems [8,9].

The spin Hall effect (SHE) [10] is a commonly used mechanism to generate a spin-polarized current and, combined with STT, to inject magnons [11–13]. The combination of both effects is also referred to as the spin-orbit torque (SOT) effect [14] and often studied in yttrium iron garnet/platinum (YIG/Pt) [15–18].

In parallel, macroscopic quantum states in the form of magnon Bose-Einstein condensates (BECs) are intensively investigated [19–24], in particular, the spontaneous coherency of the magnon BEC as an interference pattern [25] and supercurrents under a thermal gradient [26].

Recently, we found another approach using the rapid cooling (RC) mechanism to trigger the BEC formation, realized in microsized YIG/Pt structures [24]. A short DC heating pulse applied to the Pt layer resulted in Joule heating, increasing the phonon and the magnon populations. After pulse termination, the phonon temperature decreases rapidly, resulting in an overpopulation of the magnon system. Suppose the number of the so-created excess magnons is large enough. In that case, the magnon redistribution to the bottom increases the chemical potential up to a critical value, and, in turn, the formation of a magnon BEC is triggered [24].

We further discussed the combination of the SOT effect and the RC mechanism [27], demonstrating that the SOT effect can control the magnon BEC formation. Using a short pulse duration of 100 ns overcompensating the effective damping, an overpopulation at the bottom of the magnon spectrum was induced. Still, the pulses were short enough to prevent the formation of auto-oscillations in the form of a bullet mode in the current density range of interest [16,27,28]. As a result, the magnon population in a broad frequency range at the bottom increased, shifting the threshold current of BEC formation.

Here, we investigate the effect of the RC mechanism after reaching a quasistationary auto-oscillation regime driven by the SOT effect. In accordance with recent studies [16,28], we observe quasistationary auto-oscillations for the longer pulse duration used. In particular, bullet mode excitation is observed, and we find that excess magnons generated by the RC effect are redistributed to the previously STT-driven states, stabilizing the bullet mode.

Figure 1 depicts the investigated structure and the experimental setup. The structure consists of a 2-μm-broad waveguide, fabricated employing argon ion milling from a 34-nm-thick liquid phase epitaxial (LPE)-grown YIG film [29,30]. On top of the waveguide, a 3-μm-long and 7-nm-thick Pt layer is deposited using an rf-sputtering technique. Via electron beam evaporation, Ti/Au leads were attached to the Pt layer, resulting in an active injection area of 2 μm $\times$ 2 μm.

*mi_schne@rhrk.uni-kl.de

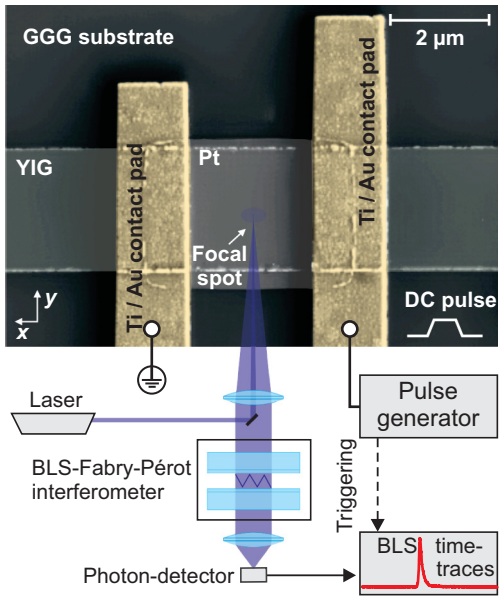

FIG. 1. Colored scanning electron microscopy (SEM) image of the investigated structure and sketch of the experimental setup. The structure consists of a 2-μm-broad and 34-nm-thick YIG waveguide. Ti/Au leads contact a 3-μm-long platinum heater (7 nm) on top. The magnon intensity under the Pt-covered region is measured using space- and time-resolved Brillouin-light-scattering spectroscopy. The DC current is parallel to the long axis of the strip. The overlap of the contacts with the Pt injector on both sides is 0.5 μm, resulting in an active injection area of 2 μm × 2 μm.

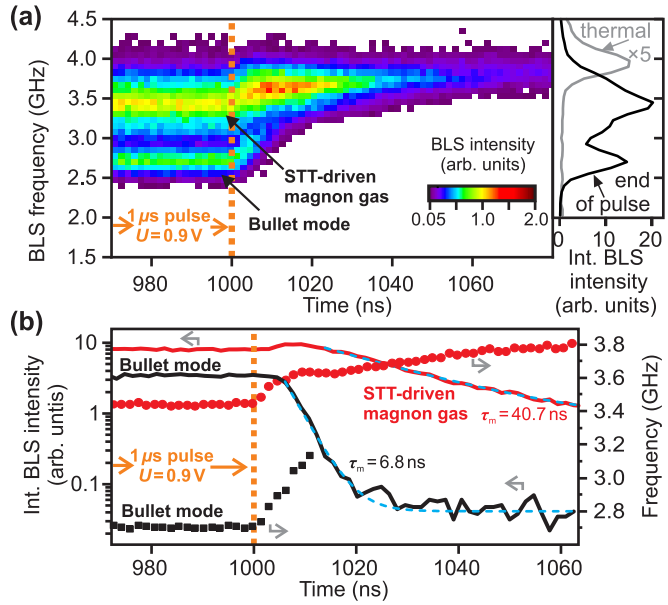

FIG. 2. (a) BLS intensity, color coded as a function of time and frequency. The dashed orange line shows the time the 1-μs-long current pulse is terminated. Right panel: Cross section for 970 ns $<$ t $<$ 1000 ns (black line) and thermal magnon spectrum (gray line). (b) Integrated BLS intensity of the bullet mode (black line) and the bottom of the magnon gas (red line) as a function of time (integration intervals 2.4 GHz $<$ f $<$ 3.0 GHz and 3.0 GHz $<$ f $<$ 4.0 GHz, respectively). Blue dashed lines are exponential fits. Red dots and black squares show the frequencies of both modes, same color code.

Standard vector network analyzer ferromagnetic resonance (VNA-FMR) measurements of two macroscopic pads of bare YIG and YIG/Pt on the same chip revealed a Gilbert damping parameter of $\alpha^{\mathrm{YIG}} = 1.83 \times 10^{-4}$ and $\alpha^{\mathrm{YIG/Pt}} = 18.1 \times 10^{-4}$, respectively, and for the YIG/Pt, a spin mixing conductance of $g^{\uparrow\downarrow} = (5.40 \pm 1.02) \times 10^{18}$ m^{-2}. An external field of $\mu_0 H_{\mathrm{ext}} = 82$ mT magnetizes the waveguide in plane along its short axis. A DC pulse generator is connected to the leads, allowing for the application of DC pulses, acting on the magnetization dynamics in the YIG via the SOT effect. Here, we focus on the case of a current polarity leading to magnon injection. In addition, the DC pulse results in Joule heating of the Pt layer, which triggers the RC mechanism after the pulse [24]. The magnetization dynamics is investigated using time- and space-resolved Brillouin light scattering (BLS) spectroscopy [31]. The light of a laser with a wavelength of $\lambda = 457$ nm is focused on the YIG guided through the transparent substrate. The inelastically scattered light carrying the information about the frequency of the magnons is analyzed by a six-pass tandem Fabry-Pérot interferometer and detected by a single photon counting module. The latter connects to a time-resolution unit triggered by the pulse generator, allowing us to investigate the time evolution of the magnon population.

To investigate the effect of the RC mechanism taking place after pulse termination, we first analyze the decaying STT-driven magnon system in the absence of a substantial contribution of the RC mechanism. As we have shown recently for a structure on the same chip, the STT-induced damping compensation sets in for current densities below the threshold of the RC-mechanism-induced condensation [27]. Although we cannot suppress the RC mechanism completely, this allows us to work in a supercritical STT regime without a significant RC-effect contribution. Moreover, the increase of the pulse duration to $\tau_{\mathrm{P}} = 1.0$ μs establishing a quasistationary auto-oscillation regime, also decreases the RC-mechanism contribution compared to our earlier studies [24,27]. A larger area close to the Pt-covered region is heated up, reducing the heat dissipation efficiency. For the particular structure and applied field, we find the threshold of the STT-driven damping compensation as $U_{\mathrm{th}}^{\mathrm{STT}} = 0.87$ V (see Supplemental Material [32]). Figure 2(a) shows the BLS intensity as a function of time and frequency for a voltage of $U = 0.9$ V (see Supplemental Material for the whole pulse duration [32]). It can be seen that the SOT effect increases the magnon population in two different frequency regions. The signal at $f \approx 3.5$ GHz corresponds to the fundamental mode: The measured frequency during the pulse is slightly below the frequency of thermal magnons, that is observed at times when no pulse is applied (1060 ns $<$ t $<$ 1080 ns). The lower frequency results from the heating and the nonlinear shift due to the large number of magnons injected. Because of the broad linewidth (see the corresponding cross section), we attribute this signal to an increased population at the bottom of the magnon gas rather than the excitation of a single mode.

In addition, we observe a peak at a lower frequency of $f = 2.7$ GHz and of a smaller linewidth (see the cross section). Due to the low frequency and linewidth, we identify this

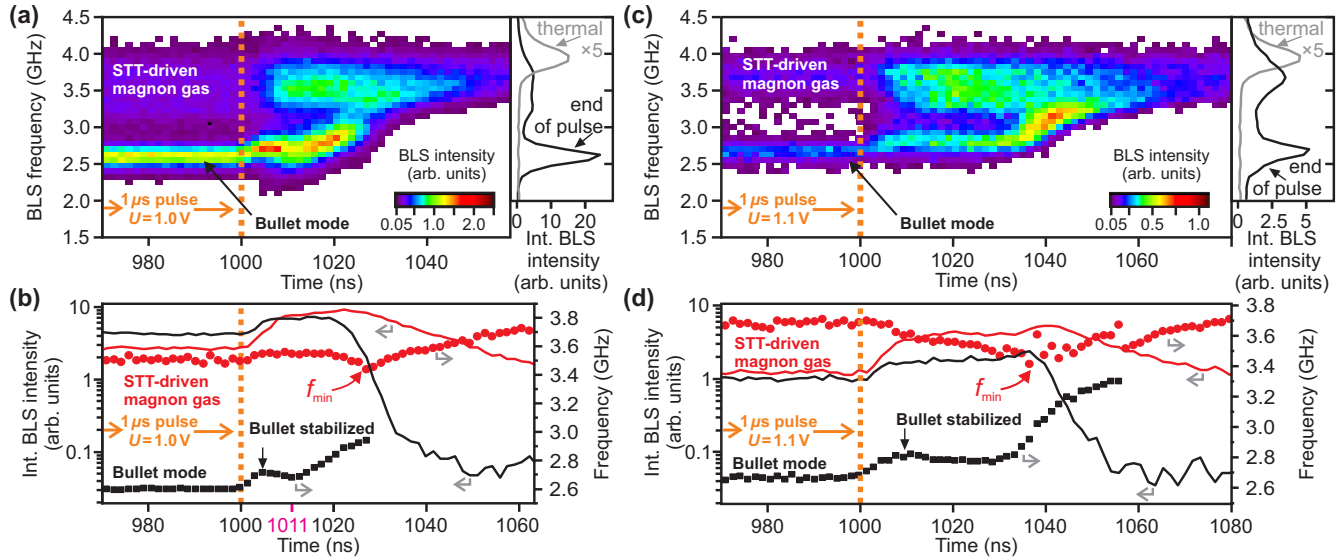

FIG. 3. (a) BLS intensity, color coded as a function of BLS frequency and time at the end and after a 1-μs-long pulse of a voltage of $U = 1.0$ V. The vertical dashed orange line indicates time of pulse termination. (b) Integrated BLS intensity of the bullet mode (black line) and the bottom of the magnon gas (red line) as a function of time. Integration intervals were 2.4 GHz $< f <$ 3.0 GHz and 3.0 GHz $< f <$ 4.0 GHz, respectively. Red dots and black squares show the frequencies of both modes, same color code. (c), (d) Same as (a), (b), but for $U = 1.1$ V.

peak as the SOT-driven excitation of the bullet mode. Such a simultaneous excitation of the low-frequency region of thermal magnons and the bullet mode has been observed in similar structures before [28]. We discuss the experimental evidence of the soliton nature in the Supplemental Material [32].

We now analyze the time evolution after pulse termination, when the RC mechanism is present. Due to the magnon redistribution processes to the bottom, we expect a deviation from an exponential decay but a relatively small RC-effect contribution due to the low voltage and long pulse duration.

Figure 2(b) shows the integrated intensities of the bottom of the magnon gas (red line) and the bullet mode (black line) as a function of time. The red dots and black squares depict the magnon gas bottom and bullet mode frequencies, respectively. Both are obtained by fitting the sum of two Gaussians. The dashed blue lines are exponential fits.

The effect of the RC mechanism is visible as an intensity increase at the bottom of the magnon gas, attributed to the magnon BEC formation process, in which the lowest-energy state of the linear magnon dispersion (for this case $f_{\mathrm{min}} \approx 3.6$ GHz) attracts the excess magnons [24]. In addition, the SOT effect creates a second attractor state in the form of a bullet mode of lower frequency (here, $f_{\mathrm{bullet}} \approx 2.7$ GHz). As a result, the bullet mode intensity stays constant after pulse termination for approximately 4 ns. Although the bullet intensity in this short time interval is constant, we observe an increasing frequency, starting instantaneously after pulse termination, which we attribute to the bullet instability. In this respect, we define the stability of the bullet mode as the state when it conserves its coherency and soliton nature, which manifests itself in the lower frequency of the bullet mode rather than in its intensity. Thus, if the frequency of the bullet mode increases, we refer to this process as to the bullet instability observed in Fig. 2(b) as the instantaneously starting frequency increase. These observations can be understood as follows: The RC mechanism redistributes magnons to both states, whereby the lowest-energy state of the linear dispersion and the SOT-driven bullet mode of lower frequency serve as natural or artificially created attractor states, respectively, but the RC mechanism is ultimately too weak to stabilize the bullet mode.

Further in time, the RC-induced redistribution finishes, and we observe an exponential decay of both modes' intensities. The exponential fits reveal amplitude lifetimes of $\tau_{\mathrm{m}} = 40.7$ ns for the magnon gas bottom and $\tau_{\mathrm{m}} = 6.8$ ns for the bullet mode. This discrepancy shows the instability of the STT-driven bullet in the absence of an external injection again.

In the following, we discuss the situation for an increased RC effect, achieved via increasing the applied voltage. Figure 3(a) shows the same data as Fig. 2, but now for $U = 1.0$ V. It can be seen that a quasistationary regime is established during the pulse, and that the bullet mode is now predominantly populated with respect to the bottom of the magnon gas and compared to the previous case. After pulse termination (orange dashed line) we now observe an increasing intensity of both modes, which shows that the excess magnons generated in the RC process redistribute to both attractor states.

To analyze the time evolution further, Fig. 3(b) shows the integrated intensities of the bottom of the magnon dispersion (red line) and of the bullet mode (black line), the frequency of the bottom of the magnon gas (red dots), and the bullet frequency (black squares).

We first focus on the bottom of the magnon gas (red line and red dots). Initially, after pulse termination, an increasing intensity and practically constant frequency are observed. For this particular case, the average frequency of the SOT-driven magnon gas (red dots at $t = 1000$ ns) is close to the final BEC frequency given by the bottom of the linear magnon dispersion (red dots at $t \approx 1025$ ns, $f_{\mathrm{min}} \approx 3.4$ GHz). Hence,

the artificially increased magnon population of the magnon gas increases the natural magnon attraction to these states. The frequency conservation is a consequence of the competition between the decreasing nonlinear shift, the cooling process, and the accumulation of magnons at the lowest-energy state of the magnon dispersion. The SOT-induced nonlinearity is the reason for the now lower final frequency of the magnon BEC with respect to the previous case of lower voltage. Finally, after approximately $t = 1030$ ns, the relaxation is visible as an increasing frequency and decreasing intensity.

We now analyze the time evolution of the bullet mode after pulse termination. Initially, the bullet mode frequency increases, analogously to the situation for $U = 0.9$ V, showing the instability of the bullet. However, the increased RC effect and the stronger attraction of the excess magnons to the now more dominantly populated bullet mode are visible as an increase in the bullet mode intensity. In the following, this increased RC effect is sufficient to stabilize the bullet, and we observe a decreasing frequency once the number of redistributed magnons is high enough. Hence, two quasicoherent states coexist in the form of the RC-driven BEC and the now stabilized bullet. Following our previous findings [24], where we observed a maximum BLS intensity around 10–20 ns after pulse termination, we measure the minimum bullet frequency, noting the time of highest bullet mode stability 11 ns after the pulse. We define this time interval of practically constant frequency as the bullet mode stabilization time.

Finally, for $t > 1011$ ns, we find the bullet mode frequency increases again, which shows that the RC mechanism is now too weak to stabilize the bullet. However, despite this observed instability, the bullet mode intensity stays constant until $t \approx 1020$ ns, indicating that magnons are still redistributed to this artificially created attractor state. We interpret this ongoing redistribution as a thermalization process in which the magnon system transits from the auto-oscillation regime to a thermalized magnon gas. The former is given by the overpopulation of the magnon condensate and the bullet mode, and the latter quasiequilibrated state is reached via the increase in the chemical potential, increasing the magnon number at the lowest-energy state.

The situation for a higher voltage of $U = 1.1$ V is shown in Figs. 3(c) and 3(d), analogously to Figs. 3(a) and 3(b). Here, we limit the discussion to the quantitative changes: With the increased voltage, the intensity of both modes at the end of the pulse decreases, which was already observed in Ref. [27] and attributed to a decreasing spin mixing conductance with increasing temperature [33]. Furthermore, the linewidth of the bottom of the magnon gas decreased, which might be due to the ongoing mode competition, resulting in a varying mode population for different injection rates. In particular, the frequency region below $f \approx 3.5$ GHz is less populated in comparison with the situation for $U = 1.0$ V. The spectral profile of injected magnons varying with the applied DC voltage results from the changed SOT supercriticality of the distinct magnon modes defined by their different decay rates.

For the bullet, we find a stabilization time of 30 ns after pulse termination. In this time interval the bullet mode frequency exhibits a constant frequency of $f = 2.78$ GHz for $1015\ \text{ns} < t < 1030$ ns, which is higher than the stable bullet frequency at the end of the pulse of $f = 2.66$ GHz. This higher frequency of the bullet results from the lower temperature and the absence of Oersted fields after pulse termination. The bullet mode intensity increases until $t = 1040$ ns.

For the magnon gas, we observe a frequency decrease after the pulse, contrary to the previous case. The decrease starts at a higher frequency but ends up at approximately the same frequency of $f \approx 3.4$ GHz (bottom of the magnon dispersion). This initially higher frequency results from the varied spectral distribution at the end of the pulse: The now stronger populated states of the magnon gas with higher frequencies increase the average frequency at the end of the pulse [compare red dots in Figs. 3(c) and 3(d) at $t \gtrsim 1000$ ns]. As a result, excess magnons are dominantly attracted to these higher-frequency states. Since the number of redistributed excess magnons is at least three times larger after the pulse, the measured frequency is determined by the redistributed magnons. Thus, we observe that the SOT-driven increased population of these higher-frequency states attracts the excess magnons. The subsequent frequency shift is caused by the natural attraction of the excess magnons to the lowest-energy state of the dispersion (BEC formation).

Our findings show that excess magnons generated by the RC effect distributed across the whole spectral range are attracted to the bottom of the magnon gas and to the bullet mode serving as an artificial attractor state. As a result, during the process of rapid cooling, these two quasicoherent states coexist. Due to the strong localization of the bullet mode [8], we interpret this as a spatially extended condensate, in which the localized bullet is embedded.

In conclusion, we have shown that the RC mechanism after the termination of an applied DC pulse can stabilize the bullet mode, which is excited via the SOT effect acting during the pulse. Depending on the applied voltage, the otherwise instantaneously unstable bullet mode conserves its low frequency for up to 30 ns. Hence, the RC effect might serve as an additional mechanism controlling conventional spin-torque oscillators (STOs) in the pulsed regime.

Moreover, we report that the spectral profile of the already excited states determines which states are populated via the subsequent RC mechanism. We interpret this feature as a stimulated condensation: The excess magnons, as bosons, want to assemble in the already highly populated states. Due to its frequency dependence, the SOT injection populates modes in the low-frequency region. Although this low energy of the here excited states might promote this stimulated condensation, the RC mechanism might also result in the redistribution to other highly populated states, suggesting that the RC mechanism can also serve as a magnon amplification mechanism in magnonic circuits.

This research was funded by the European Research Council within the Starting Grant No. 678309 "MangonCircuits" and the Advanced Grant No. 694709 "SuperMagnonics," by the Deutsche Forschungsgemeinschaft (DFG, German Research Foundation) within the Transregional Collaborative Research Center - TRR 173 - 268565370 "Spin+X" (projects B01 and B04) and through the Project No. 271741898, and by the Austrian Science Fund (FWF) within the Project No. I 4696-N.

[1] A. V. Chumak, V. I. Vasyuchka, A. A. Serga, and B. Hillebrands, Magnon spintronics, Nat. Phys. **11**, 453 (2015).

[2] J. C. Slonczewski, Current-driven excitation of magnetic multilayers, J. Magn. Magn. Mater. **159**, L1 (1996).

[3] L. Berger, Emission of spin waves by a magnetic multilayer traversed by a current, Phys. Rev. B **54**, 9353 (1996).

[4] M. Tsoi, A. G. M. Jansen, J. Bass, W.-C. Chiang, M. Seck, V. Tsoi, and P. Wyder, Excitation of a Magnetic Multilayer by an Electric Current, Phys. Rev. Lett. **80**, 4281 (1998).

[5] V. E. Demidov, S. Urazhdin, and S. O. Demokritov, Direct observation and mapping of spin waves emitted by spin-torque nano-oscillators, Nat. Mater. **9**, 984 (2010).

[6] M. Madami, S. Bonetti, G. Consolo, S. Tacchi, G. Carlotti, G. Gubbiotti, F. Mancoff, M. A. Yar, and J. Åkerman, Direct observation of a propagating spin wave induced by spin-transfer torque, Nat. Nanotechnol. **6**, 635 (2011).

[7] T. Meyer, T. Brächer, F. Heussner, A. A. Serga, H. Naganuma, K. Mukaiyama, M. Oogane, Y. Ando, B. Hillebrands, and P. Pirro, Characterization of spin-transfer-torque effect induced magnetization dynamics driven by short current pulses, Appl. Phys. Lett. **112**, 022401 (2018).

[8] A. Slavin and V. Tiberkevich, Spin Wave Mode Excited by Spin-Polarized Current in a Magnetic Nanocontact is a Standing Self-Localized Wave Bullet, Phys. Rev. Lett. **95**, 237201 (2005).

[9] V. E. Demidov, M. Evelt, V. Bessonov, S. O. Demokritov, J. L. Prieto, M. Muñoz, J. Ben Youssef, V. V. Naletov, G. Loubens, O. Klein, M. Collet, P. Bortolotti, V. Cros, and A. Anane, Direct observation of dynamic modes excited in a magnetic insulator by pure spin current, Sci. Rep. **6**, 32781 (2016).

[10] J. E. Hirsch, Spin Hall Effect, Phys. Rev. Lett. **83**, 1834 (1999).

[11] S. Urazhdin, N. O. Birge, W. P. Pratt, and J. Bass, Current-Driven Magnetic Excitations in Permalloy-Based Multilayer Nanopillars, Phys. Rev. Lett. **91**, 146803 (2003).

[12] Y. Kajiwara, K. Harii, S. Takahashi, J. Ohe, K. Uchida, M. Mizuguchi, H. Umezawa, H. Kawai, K. Ando, K. Takanashi, S. Maekawa, and E. Saitoh, Transmission of electrical signals by spin-wave interconversion in a magnetic insulator, Nature (London) **464**, 262 (2010).

[13] S. M. Mohseni, S. R. Sani, J. Persson, T. N. A. Nguyen, S. Chung, Y. Pogoryelov, P. K. Muduli, E. Iacocca, A. Eklund, R. K. Dumas, S. Bonetti, A. Deac, M. A. Hoefer, and J. Åkerman, Spin torque–generated magnetic droplet solitons, Science **339**, 1295 (2013).

[14] A. V. Khvalkovskiy, V. Cros, D. Apalkov, V. Nikitin, M. Krounbi, K. A. Zvezdin, A. Anane, J. Grollier, and A. Fert, Matching domain-wall configuration and spin-orbit torques for efficient domain-wall motion, Phys. Rev. B **87**, 020402(R) (2013).

[15] M. Collet, X. Milly, O. d'Allivy Kelly, V. V. Naletov, R. Bernard, P. Bortolotti, J. Ben Youssef, V. E. Demidov, S. O. Demokritov, J. L. Prieto, M. Muñoz, V. Cros, A. Anane, G. Loubens, and O. Klein, Generation of coherent spin-wave modes in yttrium iron garnet microdiscs by spin-orbit torque, Nat. Commun. **7**, 10377 (2016).

[16] V. Lauer, M. Schneider, T. Meyer, T. Brächer, P. Pirro, B. Heinz, F. Heussner, B. Lägel, M. C. Onbasli, C. A. Ross, B. Hillebrands, and A. V. Chumak, Temporal evolution of auto-oscillations in an yttrium-iron-garnet/platinum microdisk driven by pulsed spin Hall effect-induced spin-transfer torque, IEEE Magn. Lett. **8**, 1 (2017).

[17] M. Haidar, P. Dürrenfeld, M. Ranjbar, M. Balinsky, M. Fazlali, M. Dvornik, R. K. Dumas, S. Khartsev, and J. Åkerman, Controlling Gilbert damping in a YIG film using nonlocal spin currents, Phys. Rev. B **94**, 180409(R) (2016).

[18] A. Hamadeh, O. d'Allivy Kelly, C. Hahn, H. Meley, R. Bernard, A. H. Molpeceres, V. V. Naletov, M. Viret, A. Anane, V. Cros, S. O. Demokritov, J. L. Prieto, M. Muñoz, G. de Loubens, and O. Klein, Full Control of the Spin-Wave Damping in a Magnetic Insulator Using Spin-Orbit Torque, Phys. Rev. Lett. **113**, 197203 (2014).

[19] S. O. Demokritov, V. E. Demidov, O. Dzyapko, G. A. Melkov, A. A. Serga, B. Hillebrands, and A. N. Slavin, Bose-Einstein condensation of quasi-equilibrium magnons at room temperature under pumping, Nature (London) **443**, 430 (2006).

[20] K. Nakata, K. A. van Hoogdalem, P. Simon, and D. Loss, Josephson and persistent spin currents in Bose-Einstein condensates of magnons, Phys. Rev. B **90**, 144419 (2014).

[21] A. A. Serga, V. S. Tiberkevich, C. W. Sandweg, V. I. Vasyuchka, D. A. Bozhko, A. V. Chumak, T. Neumann, B. Obry, G. A. Melkov, A. N. Slavin, and B. Hillebrands, Bose-Einstein condensation in an ultra-hot gas of pumped magnons, Nat. Commun. **5**, 3452 (2014).

[22] Y. Tserkovnyak, S. A. Bender, R. A. Duine, and B. Flebus, Bose-Einstein condensation of magnons pumped by the bulk spin Seebeck effect, Phys. Rev. B **93**, 100402(R) (2016).

[23] C. Safranski, I. Barsukov, H. K. Lee, T. Schneider, A. A. Jara, A. Smith, H. Chang, K. Lenz, J. Lindner, Y. Tserkovnyak, M. Wu, and I. N. Krivorotov, Spin caloritronic nano-oscillator, Nat. Commun. **8**, 117 (2017).

[24] M. Schneider, T. Brächer, D. Breitbach, V. Lauer, P. Pirro, D. A. Bozhko, H. Y. Musiienko-Shmarova, B. Heinz, Q. Wang, T. Meyer, F. Heussner, S. Keller, E. T. Papaioannou, B. Lägel, T. Löber, C. Dubs, A. N. Slavin, V. S. Tiberkevich, A. A. Serga, B. Hillebrands *et al.*, Bose-Einstein condensation of quasiparticles by rapid cooling, Nat. Nanotechnol. **15**, 457 (2020).

[25] P. Nowik-Boltyk, O. Dzyapko, V. E. Demidov, N. G. Berloff, and S. O. Demokritov, Spatially non-uniform ground state and quantized vortices in a two-component Bose-Einstein condensate of magnons, Sci. Rep. **2**, 482 (2012).

[26] D. A. Bozhko, A. A. Serga, P. Clausen, V. I. Vasyuchka, F. Heussner, G. A. Melkov, A. Pomyalov, V. S. L'vov, and B. Hillebrands, Supercurrent in a room-temperature Bose–Einstein magnon condensate, Nat. Phys. **12**, 1057 (2016).

[27] M. Schneider, D. Breitbach, R. Serha, Q. Wang, A. A. Serga, A. N. Slavin, V. S. Tiberkevich, B. Heinz, B. Lägel, T. Brächer, C. Dubs, S. Knauer, O. V. Dobrovolskiy, P. Pirro, B. Hillebrands, and A. V. Chumak, Control of the Bose-Einstein condensation of magnons by the spin-Hall effect, arXiv:2102.13481.

[28] B. Divinskiy, V. E. Demidov, S. Urazhdin, R. Freeman, A. B. Rinkevich, and S. O. Demokritov, Controllable excitation of quasi-linear and bullet modes in a spin-Hall nano-oscillator, Appl. Phys. Lett. **114**, 42403 (2019).

[29] C. Dubs, O. Surzhenko, R. Thomas, J. Osten, T. Schneider, K. Lenz, J. Grenzer, R. Hübner, and E. Wendler, Low damping and microstructural perfection of sub-40nm-thin yttrium iron garnet films grown by liquid phase epitaxy, Phys. Rev. Materials **4**, 024416 (2020).

[30] B. Heinz, T. Brächer, M. Schneider, Q. Wang, B. Lägel, A. M. Friedel, D. Breitbach, S. Steinert, T. Meyer, M. Kewenig, C. Dubs, P. Pirro, and A. V. Chumak, Propagation of spin-wave packets in individual nanosized yttrium iron garnet magnonic conduits, Nano Lett. **20**, 4220 (2020).

[31] T. Sebastian, K. Schultheiss, B. Obry, B. Hillebrands, and H. Schultheiss, Micro-focused Brillouin light scattering: Imaging spin waves at the nanoscale, Front. Phys. **3**, 35 (2015).

[32] See Supplemental Material at http://link.aps.org/supplemental/10.1103/PhysRevB.104.L140405 for the damping-compensation-threshold determination, details on the BLS spectra, the bullet mode excitation and stabilization in a longitudinally magnetized waveguide, and the bullet mode localization.

[33] K.-i. Uchida, T. Kikkawa, A. Miura, J. Shiomi, and E. Saitoh, Quantitative Temperature Dependence of Longitudinal Spin Seebeck Effect at High Temperatures, Phys. Rev. X **4**, 041023 (2014).